atmosphere

MDPI

Article

Moisture Sources for the Precipitation of Tropical-like Cyclones in the Mediterranean Sea: A Case of Study

Patricia Coll-Hidalgo [1,2], Albenis Pérez-Alarcón [1,3] and Raquel Nieto [1,*]

[1] Centro de Investigación Mariña, Environmental Physics Laboratory (EPhysLab), Universidade de Vigo, Campus As Lagoas s/n, 32004 Ourense, Spain
[2] Departamento de Meteorología, Empresa Cubana de Navegación Aérea, La Habana 10800, Cuba
[3] Departamento de Meteorología, Instituto Superior de Tecnologías y Ciencias Aplicadas, Universidad de La Habana, La Habana 10400, Cuba
* Correspondence: rnieto@uvigo.es

Abstract: Tropical-like cyclones (TLCs) are hybrid low-pressure systems formed over the Mediterranean Sea, showing the characteristics of tropical and extratropical cyclones. The literature review revealed that several studies have focused on determining the physical mechanisms that favour their formation; however, their rainfall has received little attention. In this study, we attempted to identify the origin of the precipitation produced by TLCs through a Lagrangian approach based on the analysis of moisture sources for the TLC Qendresa from 6 to 9 November 2014. For the Lagrangian analysis, we used the trajectories of air parcels from the global outputs of the FLEXPART model fed by the ERA-5 reanalysis provided by the European Centre for Medium-Range Weather Forecast and backtracked those parcels that precipitated within the outer radius of the storm up to 10 days. Our results showed that the moisture mainly came from the western Mediterranean Sea, Northern Africa, the central Mediterranean Sea, Western Europe, the eastern North Atlantic, and the eastern Mediterranean Sea with contributions of 35.09%, 27.6%, 18.62%, 10.40%, 6.79%, and 1.5%, respectively. The overall large-scale conditions for the genesis of Qendresa agreed with previous climatological studies. Therefore, our findings contribute to the understanding of precipitation associated with TLCs. Future studies will focus on a climatological analysis of the origin of rainfall produced by these hybrid cyclones.

Keywords: tropical-like cyclones; Mediterranean Sea; moisture sources; precipitation; Lagrangian approach

Citation: Coll-Hidalgo, P.; Pérez-Alarcón, A.; Nieto, R. Moisture Sources for the Precipitation of Tropical-like Cyclones in the Mediterranean Sea: A Case of Study. *Atmosphere* **2022**, *13*, 1327. https://doi.org/10.3390/atmos13081327

Academic Editor: Kostas Lagouvardos

Received: 26 July 2022
Accepted: 18 August 2022
Published: 20 August 2022

1. Introduction

The Mediterranean Region (MR) is home to the genesis of several cyclones every year [1–3]. It is limited by the box from 9° W to 42° E and from 27° N to 48° N [3] and includes the Mediterranean Sea, Northern Africa, Southern Europe, and the Middle East, as shown in Figure 1. Although extratropical cyclones (ECs) are more frequent due to the baroclinic instability, mesoscale vortices showing characteristics of ECs and tropical cyclones (TCs) also occur over the MR [4–6]. These hybrid cyclones, known as Mediterranean hurricanes (medicanes) or tropical-like cyclones (TLCs), are responsible for hazardous consequences along the Mediterranean coast [7], mainly caused by their associated heavy rainfall, strong winds, and induced storm surge [4,8,9].

Several authors (e.g., [10–12]) have addressed that TLCs form the tropical transition of a baroclinic structure, i.e., frontal wave, remnant frontal zone, and a weak EC. Miglietta and Rotunno [13] listed the characteristics of a mature TLC: (i) warm core in the lower troposphere, (ii) central region free of clouds (the eye), (iii) weak vertical wind shear, (iv) strong rotation around the centre, (v) formation of spiral bands, (vi) horizontal extension of a few hundred kilometres, and (vii) exceptional intensity reaching hurricane strength. Furthermore, contrary to TCs, the lifetime of TLCs is limited to a few days due to the small extension of the Mediterranean Sea [13,14], which is their principal source of energy.

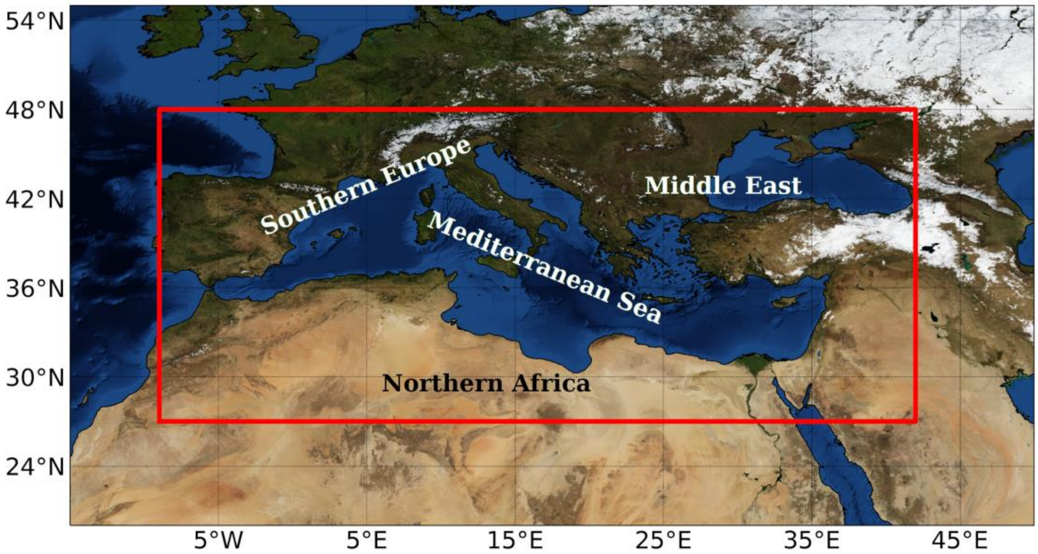

Figure 1. Mediterranean Region (red box) limited from 9° W to 42° E and from 27° N to 48° N.

Under the baroclinic conditions in which TLCs form, the weak vertical wind shear required for their development is often unusual. Therefore, the frequency of occurrence of TLCs is low, with approximately 1.5 TLC per year [7,15–17]. Likewise, the TLC season is defined from August to July of the following year [7,16], with the highest frequency from November to February [7]. Some authors (e.g., [15,18,19]) have projected that the intensity and frequency of TLCs could increase under a warming climate.

Several studies focused on TLCs have investigated the large-scale and local-scale factors for their genesis and development based on numerical simulations and climatological analysis from reanalysis datasets [20–24]. Emanuel [20] proposed that the wind-induced surface heat exchange can explain the genesis and maintenance of TLCs, but recently, Mazza et al. [12] suggested that the seclusion by colder air during the extratropical stage leads to the development of the warm core. Fita et al. [21] used a cloud-resolving model to investigate the TLC genesis and development, while Romero and Emanuel [15] used synthetic tracks of TLCs to project their future changes. Moreover, Tous and Romero [5] focused their work on the meteorological environments linked to TLCs. Miglietta et al. [6] and Comellas et al. [25] performed numerical experiments using Advanced Research Weather Research and Forecasting (WRF-ARW) to investigate the influence of physics parameterization schemes on simulations of TLCs. Nastos et al. [17] studied the interannual distribution of TLCs based on the daily average and anomalies of synoptic patterns. In addition, Zimbo et al. [26] analysed the synoptic conditions that favoured the formation and intensification of TLC Ianos from 15 to 20 September 2020, which is the most intense TLC on record [27,28].

A set of studies by Flaounas et al. [29–32] investigated the rainfall produced by Mediterranean cyclones (medcyclones), founding a relationship between the dynamic and thermodynamics process favouring heavy precipitation and cyclone intensity. Likewise, Pfahl et al. [33] noted that cyclones caused more than 90% of extreme rainfall on the Mediterranean coasts. More related to the precipitation produced by TLCs, Claud et al. [34] characterized its precipitation fields using satellite microwave observations, and Flaounas et al. [32] highlighted that TLCs tend to produce high rainfall amounts. Zhang et al. [7] examined the extreme precipitation from TLCs using the ERA-5 reanalysis [35] provided by the European Centre for Medium-Range Weather Forecasts (ECMWF) and found that rainfall totals increase from the centre to ~0.8 degrees and, then, decrease. Additionally, TLCs are responsible for 2–5% of all the extreme precipitation events in the MR from 1979 to 2017 [7]. Most recently, D'Adderio et al. [28] analysed the precipitation structure of Ianos using satellite observations, revealing notable differences in the rainband precipitation structure between the development and mature stages.

Nevertheless, where is the origin of the atmospheric humidity for the precipitation associated with TLCs? Previously, Flaounas et al. [32] applied a Lagrangian approach to identify the remote water sources for the precipitation of medcyclones. This work aims to provide new elements to address this question by investigating the moisture sources for the rainfall produced by the TLC Qendresa, which occurred from 6 to 9 November 2014. Qendresa was detected over the Sicilian channel, affecting the Islands of Lampedusa, Pantelleria, and Malta. It reached one-minute sustained winds of about 110 km/h and a minimum central pressure of 978 hPa [36,37]. While wind gusts at 135 km/h were recorded in Lampedusa, Linosa, the weather station of Buġibba in Malta registered gusts exceeding ~153 km/h. Qendresa caused three fatalities in Italy and heavy precipitation higher than 100 mm in 24 h in Malta and Sicily [37], as well as strong winds produced high waves of about 3 m or more [38]. To identify the origin of moisture associated with Qendresa, we backtracked the atmospheric humidity that precipitated over its location during its lifetime by applying the Lagrangian moisture source diagnostic method proposed by Sodemann et al. [39].

The rest of this paper includes the description of the datasets, the tracking algorithm of Qendresa and the Lagrangian moisture source tracking method in Section 2. The results are given in Section 3. Meanwhile, Section 4 summarises the main findings of this study.

2. Materials and Methods

2.1. Data

We used several three-dimensional fields, i.e., wind, specific humidity, temperature, potential vorticity, and geopotential height, from the ECMWF ERA-5 reanalysis [35]. Likewise, for investigating the moisture sources for the TLC Qendresa, we also analysed the eastward/northward vertically integrated moisture flux (VIMF), horizontal 10 m wind, convective precipitation, sensible heat flux, and surface and mean sea level pressure (MSLP). The ERA5 reanalysis has a grid spacing of 0.25° × 0.25°, 137 vertical levels, and 1-hourly temporal resolution. This reanalysis has been recently used for studying TLCs (e.g., [7,40]). Furthermore, we estimated the precipitation produced by the study case using the Multi-Source Weighted-Ensemble Precipitation (MSWEP) database [41] with a grid spacing of 0.1° × 0.1° and 3-hourly temporal resolution. The MSWEP merges precipitation estimates from 76,747 gauge stations worldwide and satellite and reanalysis datasets and includes distributional bias corrections for improving the precipitation frequency [41].

2.2. TLC Detection and Tracking Algorithm

Several algorithms have been developed for tracking low-pressure systems [42]. Some of them are focused on track TCs (e.g., [43–46]) and many others on ECs (e.g., [47–50]). However, Gaertner et al. [51] highlighted that the method proposed by Picornell et al. [52] is suitable for identifying TLCs. Previously, De la Vara et al. [40] applied this algorithm for characterizing medicanes, while González-Alemán et al. [19] obtained medcyclone trajectories by using the MSLP and the 700 hPa wind field and, then, filtered the TLCs using the cyclone phase space method proposed by Hart [53]. Here, we searched for potential TLCs over the domain 27–48° N and 9° W–48° E (see Figure 1), in agreement with Zhang et al. [7]. We detected the critical centres at each 6-hourly time step using the MSLP minima over the 3 × 3 grid points following González-Alemán et al. [19], Picornell et al. [52], and Aragão and Porcù [54]. If the distance between two potential cyclones was less than 200 km, the one with the lowest intensity was discarded. Additionally, for paring centres in continuous time steps, a critical centre at time t + 6 h is the continuation of the trajectory if it is less than 600 km from the potential centre at time t [55]. Furthermore, following Cavicchia et al. [18], track lengths smaller than 100 km were discarded to avoid persistent stationary lows. After that, we applied the cyclone phase space method [53] for filtering TLCs. Note that this study is focused on the TLC Qendresa, so we applied the tracking method from 4 to 12 November 2014.

The selection of the area delimited by the TLC size is a critical step for identifying moisture sources for the precipitation associated with it. Zhang et al. [7] used a fixed radius of 500 km for estimating the rainfall of medicanes; however, we objectively determined the TLC size by applying the method developed by Rudeva and Gulev [48]. The outer radius identification procedure starts by constructing 36 radial legs of 1000 km from the TCL centre. Then, we considered the "critical" MSLP for a given radius as the MSLP value in the location where the first radial derivative of MSLP computed at radial spatial steps of 25 km tends to zero. If the condition was not satisfied, the MSLP at 1000 km was the critical value for that leg. Subsequently, the minimum value of all "critical" MSLPs was the last closed isobar, and by interpolating it in each radial leg, we determined the system geometry, the area of which is the sum of the areas of the 36 triangles with vertices in the centre of the system and two adjacent radial legs (see Coll-Hidalgo et al. [56] for details). Then, the TLC outer radius was the radius of the virtual circumference centred on the TLC, assuming that the area of the system geometry is approximately the area of that circumference. For further details, see Rudeva and Gulev [43].

2.3. Lagrangian Method for Backtracking Moisture

For identifying the moisture sources, we used the backward trajectories of air parcels from the Lagrangian FLEXible PARTicle dispersion model (FLEXPART v10.3) [57,58] forced with the ERA-5 reanalysis. We homogeneously divided the total atmospheric mass into approximately 30 million air parcels for the model simulations. The air parcels that precipitated over the area enclosed by the TLC outer radius (the target region) were backtracked for up to 10 days [58–62]. Note that precipitating parcels were those in which the specific humidity decreased by more than 0.1 g/kg before reaching the target region, in agreement with Läderach and Sodemann [63].

By applying the quantitative Lagrangian moisture source attribution method [39], we calculated the specific humidity changes along parcels' trajectories, considering the moisture removed by precipitation before arriving at the target region. Consequently, we translated these moisture losses into fractions discounted proportionally to all previous moisture uptake, leading to remote moisture sources contributing less and less to the final precipitation. This approach has been previously applied for identifying moisture sources for heavy rainfall in Central Europe [64], East China [65], and synoptic weather systems such as TCs [66,67], deep ECs [68], medcyclones [32], and the severe winter storm formed in March 1993 over the Gulf of Mexico [56].

3. Results and Discussion

3.1. Large-Scale Conditions Associated with the Development of TLC Qendresa

Figure 2 displays the trajectory of Qendresa from 6 November at 1800 UTC to 9 November at 0000 UTC, although the tropical characteristics appeared on 7 November, in agreement with Carrió et al. [36]. Despite the limited number of observations, Carrió et al. [36] highlighted that reports from land locations close to the cyclone path provided geographical references for Qendresa's pathway (see Figure 6a in Carrió et al. [36]). The trajectory obtained by applying the tracking method described in Section 2.2 partially agrees with in situ observations and simulated trajectories by Mylonas et al. [24] and Carrió et al. [36] using the WRF-ARW model. During its lifetime (Figure 2), the TLC affected Pantelleria, Lampedusa on the island of Linosa, then Malta, and finally, the eastern coast of Sicily before losing the tropical characteristics.

The synoptic overview (Figures 3 and 4) shows that the extension through the mid-troposphere moving southwards along Western Europe was responsible for the stronger potential vorticity (PV) advection, ranging from 8 to 10 PVU (Figure 3a,b) over the western Mediterranean Sea. The enhancement of the vorticity advection over the south of Sicily on early 7 November led to the low-level cyclogenesis. Additionally, an intense upper-level cut-off low (reaching 8 PVU) separated from the PV streamer covering Northern Europe was the principal synoptic cyclone formation precursor, as shown in Figure 3. In general, the mid-level environment favoured the aloft cold air intrusion, with temperatures below −23 °C (Figure 3a–c), relative upper PVUs, and further forced general uplifts, which are factors for TLC development [11,69,70]. Additionally, a low-level cyclonic flow was predominant from 4 November over the western Mediterranean, linked to the North Atlantic Subtropical High (NASH) and high pressures over the eastern Mediterranean (Figure 4), previously documented by Carrió et al. [36]. Furthermore, the existence of the low-level depression gives the impression of the significant role of the baroclinic instability in the TLC formation, as detailed in Pytharoulis [71].

The PV anomalies in the upper troposphere between 6 and 7 November stimulated the deepening of the cyclone [24]. Mylonas et al. [24], using the ERA-5 reanalysis, pointed out that the central pressure decreased by 10.9 hPa in 6 h, reaching a minimum pressure of 991.3 hPa. Likewise, Pytharoulis [71] found a similarly abrupt drop of the minimum pressure further to 985.5 hPa using the ECMWF analysis. Figure 4 illustrates the integrated water vapour transport (IVT) during Qendresa's lifetime. Note the warm and moist northward flow from Northern Africa to the central Mediterranean. The IVT nucleus was initially in the region enclosed by the cyclone circulation (Figure 4a–c), reinforcing the system's fronts by stimulating the convective activity along its. The landfalling in Catania, located on the eastern coast of Sicily (see Figure 2) contributed to its dissipation on 9 November. However, several hypotheses have tried to explain Qendresa's decaying (e.g., [36,71]).

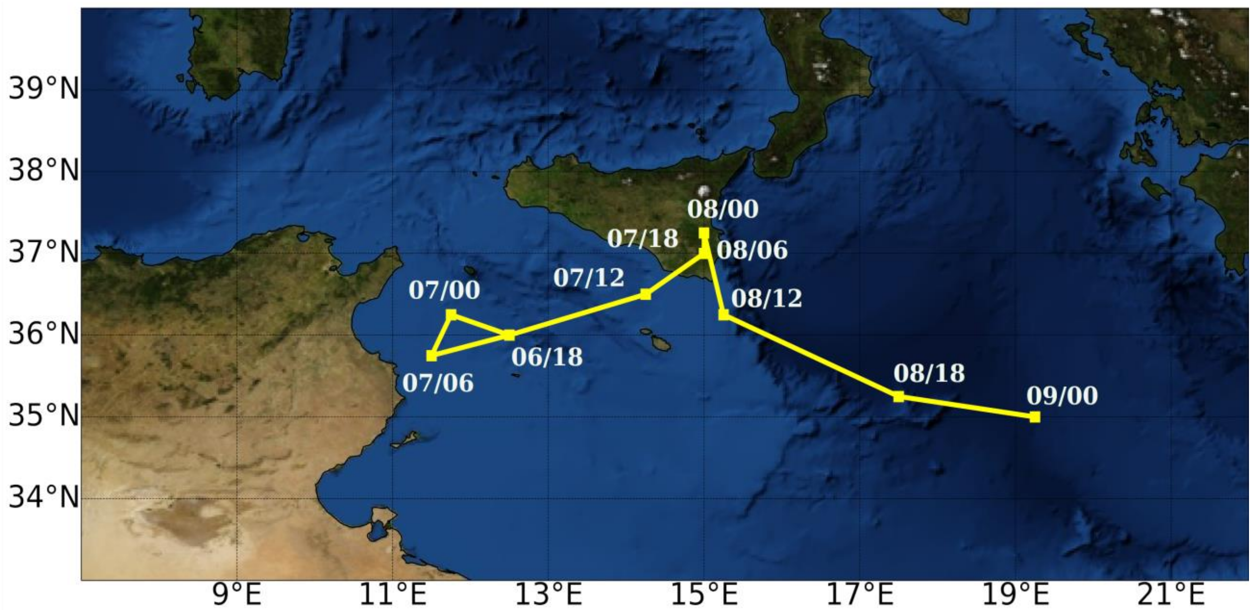

Figure 2. Trajectory of Qendresa from 6 November 2014 at 1800 UTC to 9 November 2014 at 0000 UTC. The squares denoted the 6-hourly position of the storm. Days and hours (UTC) of each Qendresa position are also plotted.

3.2. Moisture Sources for the Precipitation of Qendresa

Figure 5 shows the rain rate at a 6-hourly time step within Qendresa's outer radius from the MSWEP dataset. The intense precipitation occurred from 6 November at 1800 UTC to 7 November at 0600 UTC, with intensities higher than 6.3 mm/h over Sicily and 3.2 mm/h over Malta. According to in situ measurements, the storm produced more than 100 mm of rainfall in 24 h in Malta and Sicily [37]. From Figure 5, most of the precipitation associated with Qendresa appeared toward the northeast of the cyclone centre, in agreement with the findings of Flaounas et al. [29,31,32], who linked this behaviour with the warm conveyor belt; however, the studies by Flaounas et al. [29,31,32] included all Mediterranean cyclones. Note the higher moisture transport towards the right side of the TLC shown in Figure 4. The average rain rate around the cyclone centre ranged from 1 to 1.5 mm/h. This range agrees with the results of Zhang et al. [7], who found that TLCs produce precipitation intensities of ~1 mm/h around the centre with a pattern similar to that observed in TCs (e.g., [72,73]). It is worth noting that the decrease of the precipitation rate after Qendresa's landfall can be related to the overall reduction of the moisture transport, as revealed in the IVT pattern in Figure 5.

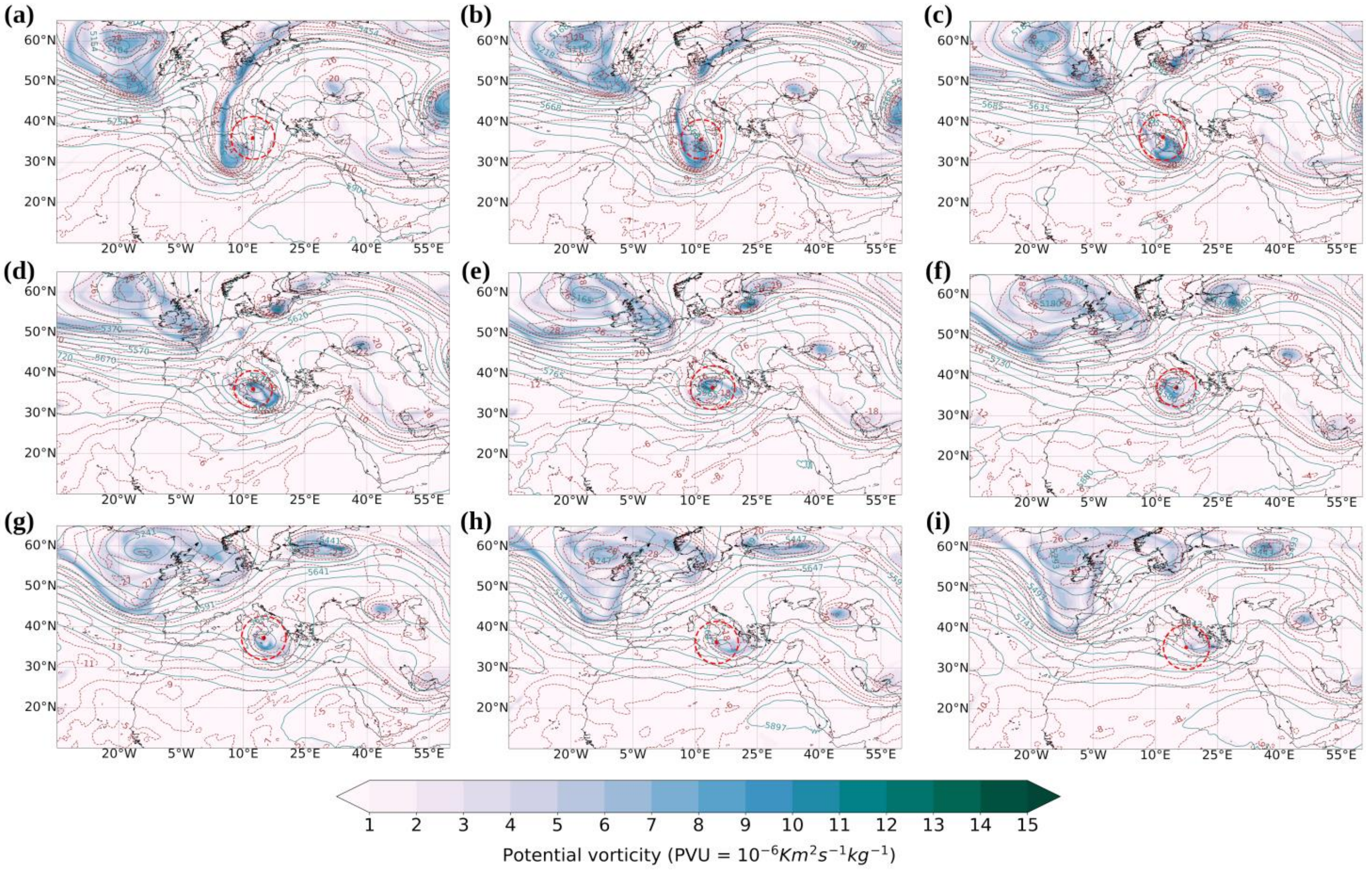

Figure 3. Potential vorticity (PVU, shaded) at 300 hPa, geopotential height (gpm, solid green line), and temperature (°C, dashed brown line) from ERA-5 reanalyses at 500 hPa during Qendresa's lifetime. (**a**) 6 November 2014 at 1800 UTC, (**b**) 7 November 2014 at 0000 UTC, (**c**) 7 November 2014 at 0600 UTC, (**d**) 7 November 2014 at 1200 UTC, (**e**) 7 November 2014 at 1800 UTC, (**f**) 8 November 2014 at 0000 UTC, (**g**) 8 November 2014 at 0600 UTC, (**h**) 8 November 2014 at 1200 UTC, and (**i**) 8 November 2014 at 1800 UTC. The dashed red circles and the red squares represent the cyclone size and centre, respectively.

To identify the origin and pathway of the moisture for Qendresa, the trajectories of the air parcels that precipitated over the TLC location followed backwards in time by applying the Lagrangian moisture source attribution method [39] are plotted in Figure 6. As previously discussed in Figure 5, the most intense precipitation occurred during the first hours of Qendresa's lifetime (Figure 5a–e). The corresponding moisture came from the northeastern North Atlantic Ocean, crossing over the Iberian Peninsula and the western Mediterranean Sea, which was driven by the convergence flux of the northern branch of the NASH and the southern branch of the deep low-pressure system located in southern Iceland (see also Figure 4). Likewise, air parcels that originated Qendresa's precipitation also travelled from the Sahel and Northern Africa, transported by the cyclonic circulation linked to the NASH and high pressures over the eastern Mediterranean Sea, in agreement with Carrió et al. [36]. A similar pattern of parcel trajectories was observed during the decay phase of Qendresa (Figure 6) after landfall on the eastern coast of Sicily (Figure 2), whereas the highest moisture uptake occurred over the eastern Mediterranean Sea.

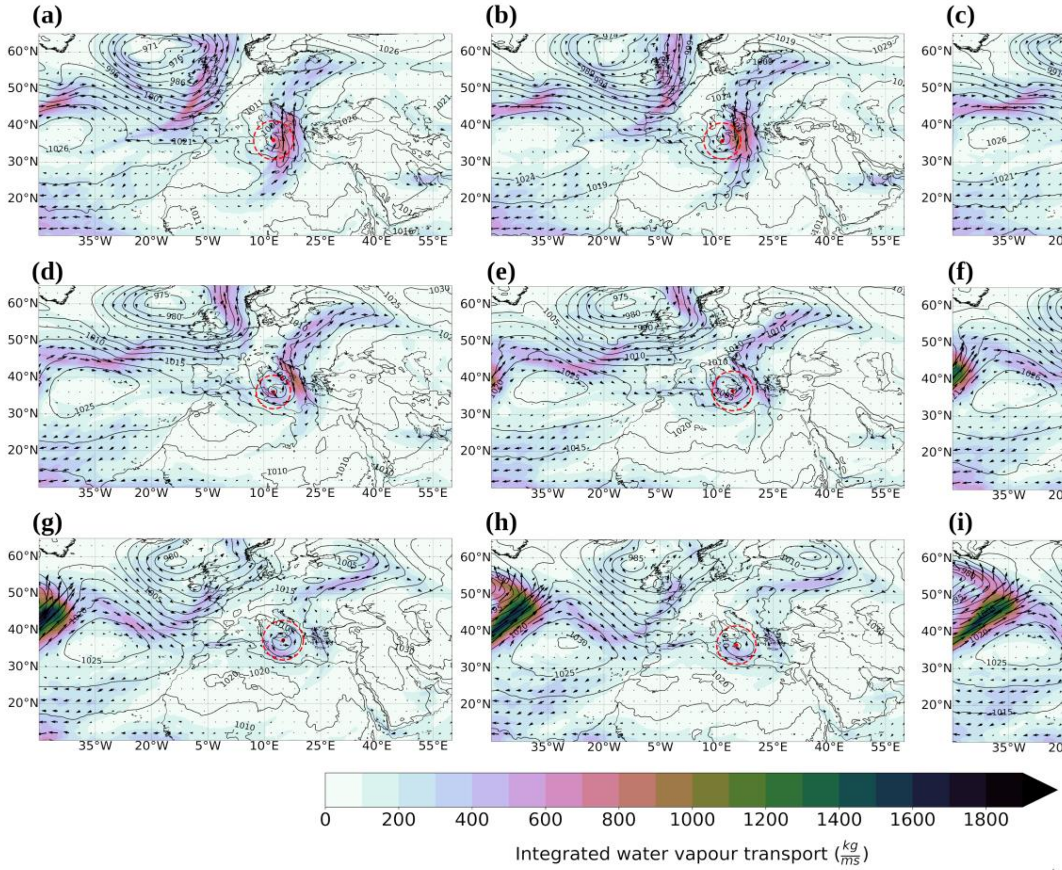

Figure 4. Integrated vertically water vapour transport (IVT, in kg/ms, shaded), vertically integrated moisture transport (VIMF, in kg/ms, arrows), and mean sea level pressure (MSLP, hPa, contour) from ERA-5 reanalysis during Qendresa's lifetime. (**a**) 6 November 2014 at 1800 UTC, (**b**) 7 November 2014 at 0000 UTC, (**c**) 7 November 2014 at 0600 UTC, (**d**) 7 November 2014 at 1200 UTC, (**e**) 7 November 2014 at 1800 UTC, (**f**) 8 November 2014 at 0000 UTC, (**g**) 8 November 2014 at 0600 UTC, (**h**) 8 November 2014 at 1200 UTC, and (**i**) 8 November 2014 at 1800 UTC. The dashed red circles and the red squares represent the cyclone size and centre, respectively.

Although air parcels manly described long northwestern–southeastern trajectories from the western North Atlantic Ocean toward Qendresa's locations, the moistening of the parcels occurred relatively close to the cyclone track. By applying the same Lagrangian approach, several authors addressed a similar behaviour in the moisture uptake pattern for ECs [56,68] and TCs [66,67]. As noted in Section 2.3, the moisture source attribution method discounted proportionally to all previous moisture uptake the precipitation en route given an objective picture of the moisture sources.

By a simple inspection of Figure 3, Figure 4, and Figure 6, the moist air parcels described trajectories bordering the extension through the mid-troposphere linked to a branch of a polar jet stream over southwestern Europe [38]. Nastos et al. [17] found by analysing the daily means of the synoptic patterns associated with the development of TLCs that they originated over regions in which cold air intrusions appear in the upper atmosphere, as we found for Qendresa (Figure 3). Based on previous findings (e.g., [10,17,74]), the cyclogenesis and intensification of TLCs are triggered by upper-tropospheric systems. Therefore, the outcome of our analysis provides an overview of the moisture sources for TLCs' precipitation.

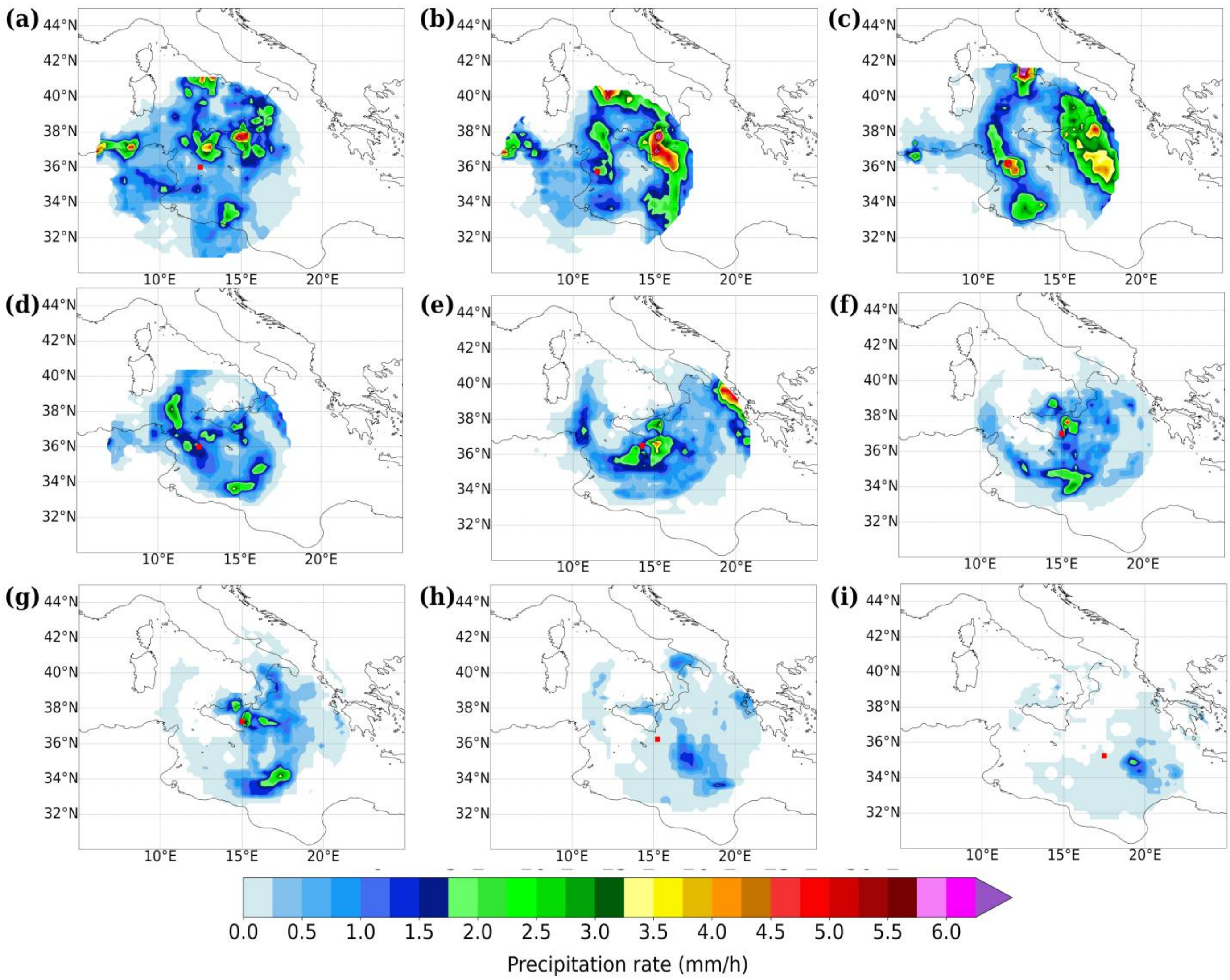

Figure 5. Precipitation rate from the Multi-Source Weighted-Ensemble Precipitation during Qendresa's lifetime. (**a**) 6 November 2014 at 1800 UTC, (**b**) 7 November 2014 at 0000 UTC, (**c**) 7 November 2014 at 0600 UTC, (**d**) 7 November 2014 at 1200 UTC, (**e**) 7 November 2014 at 1800 UTC, (**f**) 8 November 2014 at 0000 UTC, (**g**) 8 November 2014 at 0600 UTC, (**h**) 8 November 2014 at 1200 UTC, and (**i**) 8 November 2014 at 1800 UTC. The red square denotes the TLC centre.

From the analysis of the moist air parcel trajectories for the precipitation of Qendresa (Figure 6), we amassed the total contribution from the moisture sources. The overall moisture contributions are summarised in Figure 7. The moisture provided by the western Mediterranean Sea, Northern Africa, the central Mediterranean Sea, Western Europe, the eastern North Atlantic, and the eastern Mediterranean Sea accounted for 35.09%, 27.6%, 18.62%, 10.40%, 6.79%, and 1.5%, respectively. The spatial pattern of moisture uptake (Figure 7) also reveals that the atmospheric humidity mainly came from local sources, and the contributions from oceanic (terrestrial) origin represented 62% (38%) of the total moisture gained by the storm. Meanwhile, the convergence of the fluxes linked to the northern branch of the NASH and the southern portion of the low-pressure system located in southern Iceland, the polar jet stream, and the cyclonic circulation over the eastern Mediterranean Sea acted as the moisture drivers, as revealed by the VIMF pattern in Figure 7.

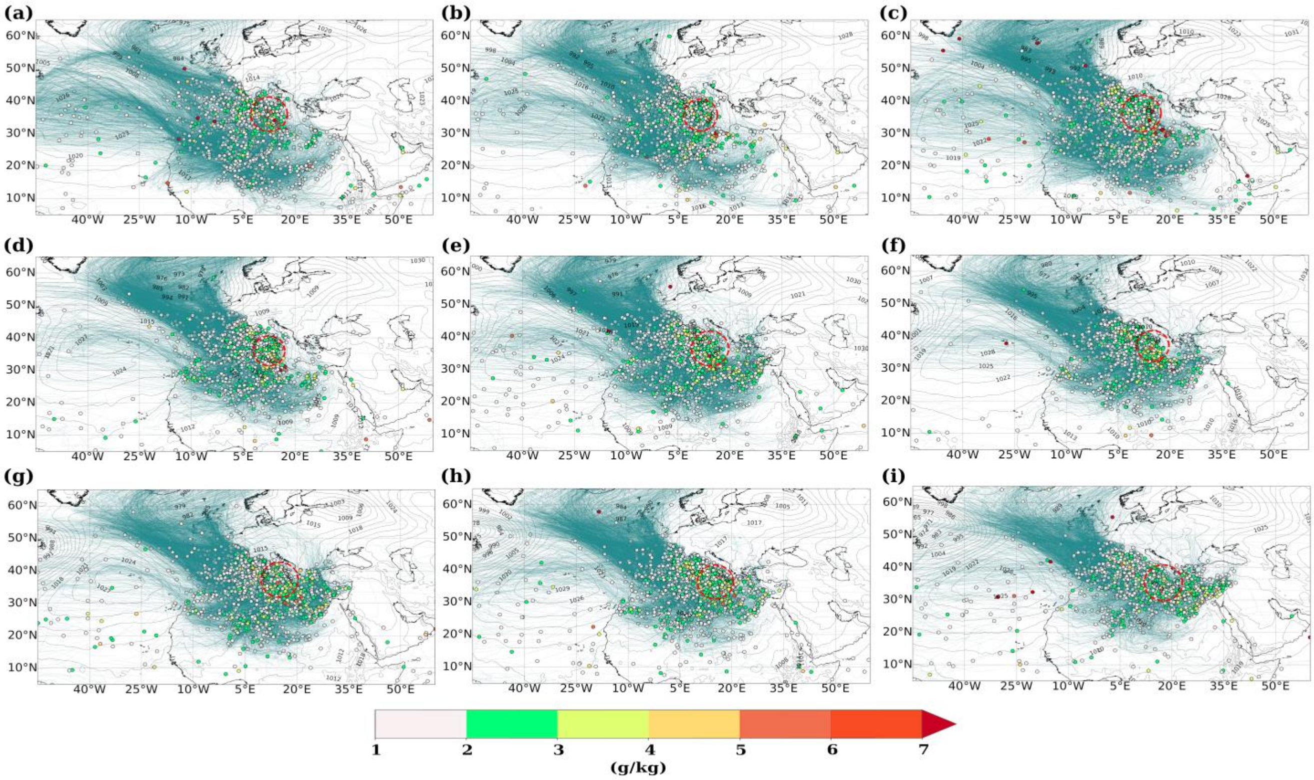

Figure 6. Trajectories of air parcels that produced the precipitation associated with Qendresa during its lifetime. (**a**) 6 November 2014 at 1800 UTC, (**b**) 7 November 2014 at 0000 UTC, (**c**) 7 November 2014 at 0600 UTC, (**d**) 7 November 2014 at 1200 UTC, (**e**) 7 November 2014 at 1800 UTC, (**f**) 8 November 2014 at 0000 UTC, (**g**) 8 November 2014 at 0600 UTC, (**h**) 8 November 2014 at 1200 UTC, and (**i**) 8 November 2014 at 1800 UTC. The mean sea level pressure (hPa) is plotted in contours; the 6 h changes in specific humidity (g/kg) are shown with coloured dots; the cyclone size is denoted by the red dashed line.

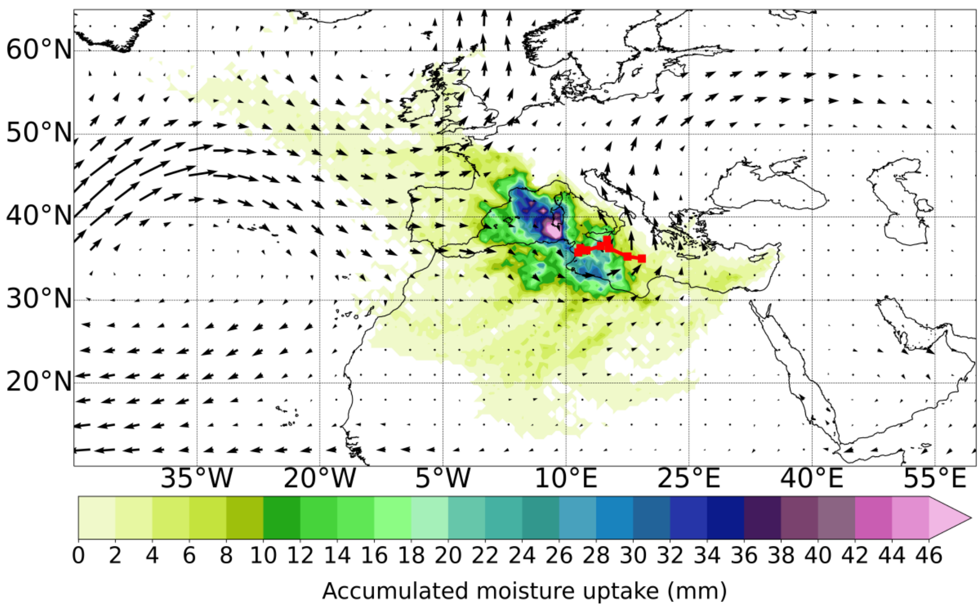

Figure 7. Accumulated moisture uptake (mm, shaded) and mean vertically integrated moisture flux (VIMF, in kg/ms, arrows) during the lifetime of Qendresa from 6 November 2014 at 1800 UTC to 9 November at 0000 UTC. The red line and squares denote the trajectory and the 6-hourly position of the storm, respectively.

4. Summary and Conclusions

Medicanes or tropical-like cyclones (TLCs) are rare hybrid cyclones formed over the Mediterranean Sea, showing the characteristics of tropical and extratropical cyclones. While the dynamics and thermodynamics mechanisms for their formation and intensification have received remarkable attention from the scientific community, little attention has been paid to the origin of their rainfall. This work aimed to identify the moisture sources for the precipitation associated with the TLC Qendresa from 6 November 2014 at 1800 UTC to 9 November 2014 at 0000 UTC by applying a Lagrangian moisture source attribution method to the air parcels' trajectories from the global outputs of the FLEXPART model fed by the ERA-5 reanalysis.

Qendresa originated on 6 November at 1800 UTC over the south-central Mediterranean Sea from an intense upper-level cut-off low linked with an extension through the mid-troposphere and then moved northeastward. During this movement, it affected Pantelleria, Lampedusa, and Malta. After landfall in eastern Sicily, it had a southeastward trajectory before dissipating over the eastern Mediterranean Sea on 9 November at 0000 UTC. During its lifetime, Qendresa produced wind gusts higher than 135 km/h in Lampedusa and 153 km/h in Malta. Additionally, the precipitation rate exhibited the highest values on the northeastern side of the storm centre, with values of about 3.2 and 6.3 mm/h over Malta and Sicily. Overall, the precipitation pattern of Qendresa agrees with the precipitation pattern of tropical cyclones.

The moisture for the precipitation produced by Qendresa was mainly driven by a branch of the polar jet stream, the convergence of surface wind associated with the circulation of the North Atlantic Subtropical High, and a deep low-pressure system located in southern Iceland, as well as a cyclonic circulation from Northern Africa towards the central Mediterranean Sea. The oceanic sources supported 62% of total moisture uptake by the storm, while the remaining 38% came from the terrestrial counterparts. Overall, the moisture provided by the western Mediterranean Sea, Northern Africa, central Mediterranean Sea, Western Europe, eastern North Atlantic, and eastern Mediterranean Sea represented 35.09%, 27.6%, 18.62%, 10.40%, 6.79%, and 1.5%, respectively. As for tropical and extratropical cyclones, the moisture mainly came from local sources close to the storm trajectory.

It is worth noting that the large-scale conditions that favoured the formation of Qendresa agree with the factors for the genesis of TLCs found by Nastos et al. [17] and Fita and Flaounas [74] in climatological studies. Therefore, this study case contributed to identifying the origin of moisture that generated the precipitation of TLCs. By including more TLCs, future works will focus on performing a climatological analysis of the moisture sources for the precipitation associated with these hybrid cyclones, the factors that control their variability, and their response to global warming.

Author Contributions: Conceptualization, R.N. and A.P.-A.; methodology, P.C.-H., A.P.-A., and R.N.; software, P.C.-H. and A.P.-A.; validation, P.C.-H. and A.P.-A.; formal analysis, P.C.-H., A.P.-A., and R.N.; investigation, P.C.-H. and A.P.-A.; resources, R.N.; data curation, P.C.-H. and A.P.-A.; writing—original draft preparation, P.C.-H. and A.P.-A.; writing—review and editing, P.C.-H.; A.P.-A., and R.N.; visualization, P.C.-H. and A.P.-A.; supervision, R.N. All authors have read and agreed to the published version of the manuscript.

Funding: This work received financial support from the LAGRIMA and SETESTRELO projects (Grants RTI2018-095772-B-I00 and PID2021-122314OB-I00, respectively) granted by the Ministerio de Ciencia, Innovación y Universidades, Spain. Partial support was received from the Xunta de Galicia under Project ED431C 2021/44 (Programa de Consolidación e Estructuración de Unidades de Investigación Competitivas (Grupos de Referencia Competitiva) and Consellería de Cultura, Educación e Universidade).

Institutional Review Board Statement: Not applicable.

Informed Consent Statement: Not applicable.

Data Availability Statement: The ERA-5 reanalysis dataset was extracted from https://www.ecmwf.int/en/forecasts/datasets/reanalysis-datasets/era5 (accessed on 11 July 2022). The Multi-Source Weighted-Ensemble Precipitation (MSWEP) dataset is freely available upon request from http://www.gloh2o.org/ (accessed on 20 April 2022). The FLEXPART model can be downloaded from https://www.flexpart.eu/wiki/FpRoadmap (accessed on 27 May 2022).

Acknowledgments: A.P.-A. thanks the University of Vigo for the Ph.D. grant program. This work was also possible thanks to the computing resources and technical support provided by CESGA (Centro de Supercomputacion de Galicia). The authors acknowledge the Copernicus Climate Change Service for providing the ECMWF reanalysis database for free.

Conflicts of Interest: The authors declare no conflict of interest.

References

1. Trigo, I.F.; Davies, T.D.; Bigg, G.R. Objective climatology of cyclones in the Mediterranean region. *J. Clim.* **1999**, *12*, 1685–1696. [CrossRef]
2. Ulbrich, U.; Leckebusch, G.C.; Pinto, J.G. Extra-tropical cyclones in the present and future climate: A review. *Theor. Appl. Climatol.* **2009**, *96*, 117–131. [CrossRef]
3. Lionello, P.; Trigo, I.F.; Gil, V.; Liberato, M.L.; Nissen, K.M.; Pinto, J.G.; Raible, C.C.; Reale, M.; Tanzarella, A.; Trigo, R.M.; et al. Objective climatology of cyclones in the Mediterranean region: A consensus view among methods with different system identification and tracking criteria. *Tellus A Dyn. Meteorol. Oceanogr.* **2016**, *68*, 29391. [CrossRef]
4. Reale, O.; Atlas, R. Tropical cyclone–like vortices in the extratropics: Observational evidence and synoptic analysis. *Wea. Forecasting* **2001**, *16*, 7–34. [CrossRef]
5. Tous, M.; Romero, R. Meteorological environments associated with medicane development. *Int. J. Climatol.* **2013**, *33*, 1–14. [CrossRef]
6. Miglietta, M.M.; Mastrangelo, D.; Conte, D. Influence of physics parameterization schemes on the simulation of a tropical-like cyclone in the Mediterranean Sea. *Atmos. Res.* **2015**, *153*, 360–375. [CrossRef]
7. Zhang, W.; Villarini, G.; Scoccimarro, E.; Napolitano, F. Examining the precipitation associated with medicanes in the high-resolution ERA-5 reanalysis data. *Int. J. Climatol.* **2021**, *41*, E126–E132. [CrossRef]
8. Moscatello, A.; Miglietta, M.M.; Rotunno, R. Numerical analysis of a Mediterranean "hurricane" over southeastern Italy. *Mon. Wea. Rev.* **2008**, *136*, 4373–4397. [CrossRef]
9. Michaelides, S.; Karacostas, T.; Sánchez, J.L.; Retalis, A.; Pytharoulis, I.; Homar, V.; Romerof, R.; Zanisc, P.; Giannakopoulose, C.; Bühl, J.; et al. Reviews and perspectives of high impact atmospheric processes in the Mediterranean. *Atmos. Res.* **2018**, *208*, 4–44. [CrossRef]
10. Chaboureau, J.P.; Pantillon, F.; Lambert, D.; Richard, E.; Claud, C. Tropical transition of a Mediterranean storm by jet crossing. *Q. J. R. Meteorol. Soc.* **2012**, *138*, 596–611. [CrossRef]
11. Cioni, G.; Malguzzi, P.; Buzzi, A. Thermal structure and dynamical precursor of a Mediterranean tropical-like cyclone. *Q. J. R. Meteorol. Soc.* **2016**, *142*, 1757–1766. [CrossRef]
12. Mazza, E.; Ulbrich, U.; Klein, R. The tropical transition of the October 1996 medicane in the western Mediterranean Sea: A warm seclusion event. *Mon. Weather Rev.* **2017**, *145*, 2575–2595. [CrossRef]
13. Miglietta, M.M.; Rotunno, R. Development mechanisms for Mediterranean tropical-like cyclones (medicanes). *Q. J. R. Meteorol. Soc.* **2019**, *145*, 1444–1460. [CrossRef]
14. Miglietta, M.M.; Laviola, S.; Malvaldi, A.; Conte, D.; Levizzani, V.; Price, C. Analysis of tropical-like cyclones over the Mediterranean Sea through a combined modelling and satellite approach. *Geophys. Res. Lett.* **2013**, *40*, 2400–2405. [CrossRef]
15. Romero, R.; Emanuel, K. Medicane risk in a changing climate. *J. Geophys. Res. Atmospheres* **2013**, *118*, 5992–6001. [CrossRef]
16. Cavicchia, L.; von Storch, H.; Gualdi, S. A long-term climatology of medicanes. *Clim. Dyn.* **2014**, *43*, 1183–1195. [CrossRef]
17. Nastos, P.T.; Papadimou, K.K.; Matsangouras, I.T. Mediterranean tropical-like cyclones: Impacts and composite daily means and anomalies of synoptic patterns. *Atmos. Res.* **2018**, *208*, 156–166. [CrossRef]
18. Cavicchia, L.; von Storch, H.; Gualdi, S. Mediterranean tropical-like cyclones in present and future climate. *J. Clim.* **2014**, *27*, 7493–7501. [CrossRef]
19. González-Alemán, J.J.; Pascale, S.; Gutierrez-Fernandez, J.; Murakami, H.; Gaertner, M.A.; Vecchi, G.A. Potential increase in hazard from Mediterranean hurricane activity with global warming. *Geophys. Res. Lett.* **2019**, *46*, 1754–1764. [CrossRef]
20. Emanuel, K. Genesis and maintenance of "Mediterranean hurricanes". *Adv. Geosci.* **2005**, *2*, 217–220. [CrossRef]
21. Fita, L.; Romero, R.; Luque, A.; Emanuel, K.; Ramis, C. Analysis of the environments of seven Mediterranean tropical-like storms using an axisymmetric, nonhydrostatic, cloud resolving model. *Nat. Hazards Earth Syst. Sci.* **2007**, *7*, 41–56. [CrossRef]
22. Conte, D.; Miglietta, M.M.; Levizzani, V. Analysis of instability indices during the development of a Mediterranean tropical-like cyclone using MSG-SEVIRI products and the LAPS model. *Atmos. Res.* **2011**, *101*, 264–279. [CrossRef]
23. Flaounas, E.; Gray, S.L.; Teubler, F. A process-based anatomy of Mediterranean cyclones: From baroclinic lows to tropical-like systems. *Weather Clim. Dyn.* **2021**, *2*, 255–279. [CrossRef]

24. Mylonas, M.P.; Douvis, K.C.; Polychroni, I.D.; Politi, N.; Nastos, P.T. Analysis of a Mediterranean Tropical-Like Cyclone. Sensitivity to WRF Parameterizations and Horizontal Resolution. *Atmosphere* **2019**, *10*, 425. [CrossRef]
25. Comellas Prat, A.; Federico, S.; Torcasio, R.C.; D'Adderio, L.P.; Dietrich, S.; Panegrossi, G. Evaluation of the Sensitivity of Medicane Ianos to Model Microphysics and Initial Conditions Using Satellite Measurements. *Remote Sens.* **2021**, *13*, 4984. [CrossRef]
26. Zimbo, F.; Ingemi, D.; Guidi, G. The Tropical-like Cyclone "Ianos" in September 2020. *Meteorology* **2022**, *1*, 29–44. [CrossRef]
27. Lagouvardos, K.; Karagiannidis, A.; Dafis, S.; Kalimeris, A.; Kotroni, V. Ianos-A hurricane in the Mediterranean. *Bull. Am. Meteorol.* **2022**, *103*, E1621–E1636. [CrossRef]
28. D'Adderio, L.P.; Casella, D.; Dietrich, S.; Sanò, P.; Panegrossi, G. GPM-CO observations of Medicane Ianos: Comparative analysis of precipitation structure between development and mature phase. *Atmos. Res.* **2022**, *273*, 106174. [CrossRef]
29. Flaounas, E.; Di Luca, A.; Drobinski, P.; Mailler, S.; Arsouze, T.; Bastin, S.; Beranger, K.; Lebeaupin Brossier, C. Cyclone contribution to the Mediterranean Sea water budget. *Clim. Dyn.* **2016**, *46*, 913–927. [CrossRef]
30. Flaounas, E.; Kelemen, F.D.; Wernli, H.; Gaertner, M.A.; Reale, M.; Sanchez-Gomez, E.; Lionello, P.; Calmanti, S.; Podrascanin, Z.; Somot, S.; et al. Assessment of an ensemble of ocean–atmosphere coupled and uncoupled regional climate models to reproduce the climatology of Mediterranean cyclones. *Clim. Dyn.* **2018**, *51*, 1023–1040. [CrossRef]
31. Flaounas, E.; Kotroni, V.; Lagouvardos, K.; Gray, S.L.; Rysman, J.-F.; Claud, C. Heavy rainfall in Mediterranean cyclones. Part I: Contribution of deep convection and warm conveyor belt. *Clim. Dyn.* **2018**, *50*, 2935–2949. [CrossRef]
32. Flaounas, E.; Fita, L.; Lagouvardos, K.; Kotroni, V. Heavy rainfall in Mediterranean cyclones, Part II: Water budget, precipitation efficiency and remote water sources. *Clim. Dyn.* **2019**, *53*, 2539–2555. [CrossRef]
33. Pfahl, S.; Madonna, E.; Boettcher, M.; Joos, H.; Wernli, H. Warm conveyor belts in the ERA-Interim dataset (1979–2010). Part II: Moisture origin and relevance for precipitation. *J. Clim.* **2014**, *27*, 27–40. [CrossRef]
34. Claud, C.; Alhammoud, B.; Funatsu, B.M.; Chaboureau, J.P. Mediterranean hurricanes: Large-scale environment and convective and precipitating areas from satellite microwave observations. *Nat. Hazards Earth Syst. Sci.* **2010**, *10*, 2199–2213. [CrossRef]
35. Hersbach, H.; Bell, B.; Berrisford, P.; Hirahara, S.; Horányi, A.; Muñoz-Sabater, J.; Nicolas, J.; Peubey, C.; Radu, R.; Schepers, D.; et al. The ERA5 global reanalysis. *Q. J. R. Meteorol. Soc.* **2020**, *146*, 1999–2049. [CrossRef]
36. Carrió, D.S.; Homar, V.; Jansa, A.; Romero, R.; Picornell, M.A. Tropicalization process of the 7 November 2014 Mediterranean cyclone: Numerical sensitivity study. *Atmos. Res.* **2017**, *197*, 300–312. [CrossRef]
37. EUMETSAT. A Medicane (MEDIterranean hurriCANE) or Tropical-Like Cyclone (TLC) Brought Severe Weather to Parts of the Mediterranean in Early November. Available online: https://web.archive.org/web/20201107205936/https://www.eumetsat.int/website/home/Images/ImageLibrary/DAT_2412479.html (accessed on 22 July 2022).
38. Kerkmann, J.; Higgins, M.; Lancaster, S.; Roesli, H.P.; Tsiniari, E.; Sachweh, M.; EUMETSAT. Medicane Qendresa Hits Malta and Sicily. 2014. Available online: https://www.eumetsat.int/medicane-qendresa-hits-Malta-and-Sicily (accessed on 17 July 2022).
39. Sodemann, H.; Schwierz, C.; Wernli, H. Interannual variability of Greenland winter precipitation sources: Lagrangian moisture diagnostic and north Atlantic oscillation influence. *J. Geophys. Res.* **2008**, *113*, D03107. [CrossRef]
40. De la Vara, A.; Gutiérrez-Fernández, J.; González-Alemán, J.J.; Gaertner, M.A. Characterization of medicanes with a minimal number of geopotential levels. *Int. J. Climatol.* **2021**, *41*, 3300–3316. [CrossRef]
41. Beck, H.E.; Wood, E.F.; Pan, M.; Fisher, C.K.; Miralles, D.G.; Van Dijk, A.I.; McVicar, T.R.; Adler, R.F. MSWEP V2 global 3-hourly 0.1 precipitation: Methodology and quantitative assessment. *Bull. Am. Meteorol. Soc.* **2019**, *100*, 473–500. [CrossRef]
42. Ullrich, P.A.; Zarzycki, C.M. TempestExtremes: A framework for scale-insensitive pointwise feature tracking on unstructured grids. *Geosci. Model Dev.* **2017**, *10*, 1069–1090. [CrossRef]
43. Walsh, K.J.E.; Nguyen, K.C.; McGregor, J.L. Fine-resolution regional climate model simulations of the impact of climate change on tropical cyclones near Australia. *Clim. Dyn.* **2004**, *22*, 47–56. [CrossRef]
44. Zhao, M.; Held, I.M.; Lin, S.J.; Vecchi, G.A. Simulations of global hurricane climatology, interannual variability, and response to global warming using a 50-km resolution GCM. *J. Clim.* **2009**, *22*, 6653–6678. [CrossRef]
45. Murakami, H.; Mizuta, R.; Shindo, E. Future changes in tropical cyclone activity projected by multi-physics and multi-SST ensemble experiments using the 60-km-mesh MRI-AGCM. *Clim. Dyn.* **2012**, *39*, 2569–2584. [CrossRef]
46. Bacmeister, J.T.; Suarez, M.J.; Robertson, F.R.; Wehner, M.F.; Neale, R.B.; Gettelman, A.; Hannay, C.; Lauritzen, P.H.; Caron, J.M.; Truesdale, J.E. Exploratory high-resolution climate simulations using the Community Atmosphere Model (CAM). *J. Clim.* **2014**, *27*, 3073–3099. [CrossRef]
47. Pinto, J.G.; Spangehl, T.; Ulbrich, U.; Speth, P. Sensitivities of a cyclone detection and tracking algorithm: Individual tracks and climatology. *Meteorol. Z.* **2005**, *14*, 823–838. [CrossRef]
48. Rudeva, I.; Gulev, S.K. Climatology of cyclone size characteristics and their changes during the cyclone life cycle. *Mon. Weather Rev.* **2007**, *135*, 2568–2587. [CrossRef]
49. Raible, C.C.; Della-Marta, P.M.; Schwierz, C.; Wernli, H.; Blender, R. Northern Hemisphere extratropical cyclones: A comparison of detection and tracking methods and different reanalyses. *Mon. Weather Rev.* **2008**, *136*, 880–897. [CrossRef]
50. Neu, U.; Akperov, M.G.; Bellenbaum, N.; Benestad, R.; Blender, R.; Caballero, R.; Cocozza, A.; Dacre, H.F.; Feng, Y.; Fraedrich, K.; et al. IMILAST: A community effort to intercompare extratropical cyclone detection and tracking algorithms. *Bull. Am. Meteorol Soc.* **2013**, *94*, 529–547. [CrossRef]

51. Gaertner, M.Á.; González-Alemán, J.J.; Romera, R.; Domínguez, M.; Gil, V.; Sánchez, E.; Gallardo, C.; Miglietta, M.M.; Walsh, K.J.E.; Sein, D.V.; et al. Simulation of medicanes over the Mediterranean Sea in a regional climate model ensemble: Impact of ocean–atmosphere coupling and increased resolution. *Clim. Dyn.* **2018**, *51*, 1041–1057. [CrossRef]
52. Picornell, M.A.; Jansa, A.; Genovés, A.; Campins, J. Automated database of mesocyclones from the HIRLAM (INM)-0.5° analyses in the western Mediterranean. *Int. J. Climatol.* **2001**, *21*, 335–354. [CrossRef]
53. Hart, R.E. A cyclone phase space derived from thermal wind and thermal asymmetry. *Mon. Wea. Rev.* **2003**, *131*, 585–616. [CrossRef]
54. Aragão, L.; Porcù, F. Cyclonic activity in the Mediterranean region from a high-resolution perspective using ECMWF ERA5 dataset. *Clim. Dyn.* **2022**, *58*, 1293–1310. [CrossRef]
55. Cavicchia, L.; von Storch, H. The simulation of medicanes in a high-resolution regional climate model. *Clim. Dyn.* **2012**, *39*, 2273–2290. [CrossRef]
56. Coll-Hidalgo, P.; Pérez-Alarcón, A.; Gimeno, L. Origin of Moisture for the Precipitation Produced by the Exceptional Winter Storm Formed over the Gulf of Mexico in March 1993. *Atmosphere* **2022**, *13*, 1154. [CrossRef]
57. Stohl, A.; Forster, C.; Frank, A.; Seibert, P.; Wotawa, G. Technical note: The Lagrangian particle dispersion model FLEXPART version 6.2. *Atmos. Chem. Phys.* **2005**, *5*, 2461–2474. [CrossRef]
58. Pisso, I.; Sollum, E.; Grythe, H.; Kristiansen, N.I.; Cassiani, M.; Eckhardt, S.; Arnold, D.; Morton, D.; Thompson, R.L.; Groot Zwaaftink, C.D.; et al. The Lagrangian particle dispersion model FLEXPART version 10.4. *Geosci. Model Dev.* **2019**, *12*, 4955–4997. [CrossRef]
59. Numaguti, A. Origin and recycling processes of precipitating water over the Eurasian continent: Experiments using an atmospheric general circulation model. *J. Geophys. Res.* **1999**, *104*, 1957–1972. [CrossRef]
60. Gimeno, L.; Eiras-Barca, J.; Durán-Quesada, A.M.; Dominguez, F.; van der Ent, R.; Sodemann, H.; Sánchez-Murillo, R.; Nieto, R.; Kirchner, J.W. The residence time of water vapour in the atmosphere. *Nat. Rev. Earth Environ.* **2021**, *2*, 558–569. [CrossRef]
61. Wang, N.; Zeng, X.M.; Zheng, Y.; Zhu, J.; Jiang, S. The atmospheric moisture residence time and reference time for moisture tracking over China. *J. Hydrometeorol.* **2018**, *19*, 1131–1147. [CrossRef]
62. van der Ent, R.J.; Tuinenburg, O.A. The residence time of water in the atmosphere revisited. *Hydrol. Earth Syst. Sci.* **2017**, *21*, 779–790. [CrossRef]
63. Läderach, A.; Sodemann, H. A revised picture of the atmospheric moisture residence time. *Geophys. Res. Lett.* **2016**, *43*, 924–933. [CrossRef]
64. Krug, A.; Aemisegger, F.; Sprenger, M.; Ahrens, B. Moisture sources of heavy precipitation in Central Europe in synoptic situations with Vb-cyclones. *Clim. Dyn.* **2022**. [CrossRef]
65. Shi, Y.; Jiang, Z.; Liu, Z.; Li, L. A Lagrangian analysis of water vapor sources and pathways for precipitation in East China in different stages of the East Asian summer monsoon. *J. Clim.* **2020**, *33*, 977–992. [CrossRef]
66. Pérez-Alarcón, A.; Sorí, R.; Fernández-Alvarez, J.C.; Nieto, R.; Gimeno, L. Where does the moisture for North Atlantic tropical cyclones come from? *J. Hydrometeorol.* **2022**, *23*, 457–472. [CrossRef]
67. Pérez-Alarcón, A.; Coll-Hidalgo, P.; Fernández-Alvarez, J.C.; Sorí, R.; Nieto, R.; Gimeno, L. Moisture sources for precipitation associated with major hurricanes during 2017 in the North Atlantic basin. *J. Geophys. Res. Atmos.* **2022**, *127*, e2021JD035554. [CrossRef]
68. Papritz, L.; Aemisegger, F.; Wernli, H. Sources and transport pathways of precipitating waters in cold-season deep North Atlantic cyclones. *J. Atmos. Sci.* **2021**, *78*, 3349–3368. [CrossRef]
69. Miglietta, M.M.; Cerrai, D.; Laviola, S.; Cattani, E.; Levizzani, V. Potential vorticity patterns in Mediterranean "hurricanes". *Geophys. Res. Lett.* **2017**, *44*, 2537–2545. [CrossRef]
70. Homar, V.; Romero, R.; Stensrud, D.J.; Ramis, C.; Alonso, S. Numerical diagnosis of a small, quasi-tropical cyclone over the western Mediterranean: Dynamical vs. boundary factors. *Q. J. R. Meteorol. Soc.* **2003**, *129*, 1469–1490. [CrossRef]
71. Pytharoulis, I. Analysis of a Mediterranean tropical-like cyclone and its sensitivity to the sea surface temperatures. *Atmos. Res.* **2018**, *208*, 167–179. [CrossRef]
72. Rios-Gaona, M.F.; Villarini, G.; Zhang, W.; Vecchi, G.A. The added value of IMERG in characterizing rainfall in tropical cyclones. *Atmos. Res.* **2018**, *209*, 95–102. [CrossRef]
73. Zhang, W.; Villarini, G.; Vecchi, G.A.; Murakami, H. Rainfall from tropical cyclones: High-resolution simulations and seasonal forecasts. *Clim. Dyn.* **2019**, *52*, 5269–5289. [CrossRef]
74. Fita, L.; Flaounas, E. Medicanes as subtropical cyclones: The December 2005 case from the perspective of surface pressure tendency diagnostics and atmospheric water budget. *Q. J. R. Meteorol. Soc.* **2018**, *144*, 1028–1044. [CrossRef]